FFEMS Fatigue & Fracture of Engineering Materials & Structures
ORIGINAL CONTRIBUTION
doi: 10.1111/ffe.12563

Fatigue behaviour of dissimilar Al 5052 and Mg AZ31 resistance spot welds with Sn-coated steel interlayer

M SUN[1,2], S B BEHRAVESH[1], L WU[3], Y ZHOU[1] and H JAHED[1]

[1]*Department of Mechanical and Mechatronics Engineering, University of Waterloo, Waterloo N2l 3G1Ontario Canada*, [2]*Aerospace Research Institute of Materials and Processing Technology, Beijing 100076, China*, [3]*State Key Laboratory of Advanced Welding and Joining, Harbin Institute of Technology, Harbin 150001, China*

Received Date: 29 July 2016; Accepted Date: 13 November 2016; Published Online: 28 December 2016

ABSTRACT The fatigue property of dissimilar spot welds between an aluminium alloy (AA5052) and a magnesium alloy (AZ31) was studied in this research. The AA5052 and AZ31 coupons were resistance spot welded together by using an interlayer of Sn-coated steel between the two coupons. The fatigue test results revealed that the Mg/Al joints had the same level of fatigue strength as Mg/Mg resistance spot welds. It was found that within the life range of $N_f < 10^5$ cycles, Mg/Al welds degraded faster than Mg/Mg joints. This was attributed to the larger bending moment on the plane of fatigue failure in the Mg/Al welds. Three failure modes were observed under different cyclic loading regimes: Al/steel interfacial failure, Mg coupon failure and Al coupon failure. Fatigue fracture surface of Mg/Al welds consisted of two distinct regions: crack propagation region with brittle morphology and final rupture with ductile morphology.

Keywords fatigue of welds; resistance spot welding; Mg/Al spot weld; Sn-coated steel interlayer.

NOMENCLATURE

F	= external load on tensile-shear specimens
F_{min}, F_{max}	= minimum and maximum loads in load-controlled cyclic tests
δF	= load range
N_f	= fatigue life
R	= Load ratio

ABBREVIATIONS

EDS	= energy-dispersive X-ray spectroscopy
HCF	= high cycle fatigue
IMC	= intermetallic compound
LCF	= low cycle fatigue
SEM	= scanning electron microscope

INTRODUCTION

Under the current energy crisis, the reduction of vehicle mass is a strong demand for the automotive industry. As the lightest structural metal, magnesium (Mg) has attracted attentions in various industries, due to the high specific strength, excellent castability, machinability and sound damping capability.[1] Aluminium (Al) alloys are also extensively utilized in the automotive industry because of a range of desirable properties, for example, low density, excellent corrosion performance and high specific strength.[2,3] Thus, Mg and Al alloys are viable alternatives for steel to reduce the weight of vehicles. Several recent researches aimed at developing multimaterial automotive body structures, involving Mg and Al alloys and high-strength steels.[4,5] Therefore, welding between Mg and Al components is a critical part of the new body structures' design philosophy.

According to the Al–Mg binary phase diagram,[6] the unfavourable hard and brittle Al–Mg intermetallic

Correspondence: H. Jahed. E-mail: hjahed@uwaterloo.ca

compounds (IMCs) can be formed in the weld region during the welding process, which results in poor strength of Mg/Al welds. Several welding methods were investigated for joining Al to Mg alloys, such as laser welding,[7,8] vacuum diffusion bonding,[9,10] gas tungsten arc welding,[11] resistance spot welding,[12] ultrasonic spot welding[13,14] and friction stir welding.[15–17] Previous studies demonstrated that the Al–Mg IMCs such as Al_3Mg_2 and $Al_{12}Mg_{17}$ have a harmful effect on the strength of Mg/Al joint and could hardly be prevented during the welding process.[15,18–20] To reduce the formation of Al–Mg IMCs, an interlayer made of a third metal, such as copper, steel, cerium, titanium and nickel, was placed between Al and Mg coupons during welding. The effect of different interlayers has been investigated in a number of studies.[4,21–26] It was demonstrated that the addition of an interlayer restrained the reaction between Al and Mg, thus reduced the formation of Al–Mg IMC[4,21–26] and enhanced the joint strength. As a predominant welding method in the automotive industry, resistance spot welding been studied to make Al to Mg joints by using this technique, and several interlayers have been examined.[21,26–28] In the study of Mg/Al spot welds[27] with an interlayer of Sn-coated steel, the results showed great increase in the joint static strength compared with that of the Mg/Al direct welds (no interlayer).

Numerous studies have been performed on fatigue characterization of similar spot welds, such as steel/steel and Al/Al.[29,30] However, limited studies are available on fatigue of Mg/Mg similar spot welds. Behravesh *et al.*[31–33] investigated the fatigue behaviour of magnesium spot welds with different nugget sizes. They reported that in the low cycle fatigue (LCF) regime, the fatigue strength is enhanced by increasing the nugget size. This effect diminishes in the high cycle fatigue (HCF) regime.[31] Three failure modes were observed: Interfacial failure and coupon failure occurred in the LCF and HCF regimes, respectively, and partially interfacial failure was a transition between the two. Fatigue crack initiates close to the nugget edge in the LCF regime, but in the HCF regime, the initiation point moves farther from the nugget.[32] Comparison between spot welds of magnesium, aluminium and steel revealed that magnesium and aluminium spot welds have similar fatigue strength, while steel exhibits significantly higher strength.[33] Fatigue crack initiation life was estimated in magnesium spot welds, and it was observed that the portion of crack initiation life to total life increases from LCF to HCF regime.[33] Different fatigue models were used to predict the fatigue life of magnesium spot welds. The accuracy of these models was assessed and discussed.[33] Xiao *et al.*[34] studied the effect of fusion zone microstructure on the fatigue behaviour of magnesium spot welds. They reported that refined microstructure in the fusion zone resulted in a longer fatigue life under high cyclic load where interfacial failure occurred. Basal slip, pyramidal slip and twining were identified as the deformation mechanisms inside the fusion zone, with twinning appearing more in the welds with coarser microstructure.

A few published works are available on fatigue of magnesium dissimilar joints. Liu *et al.*[35] compared the fatigue strength of Mg/steel spot-welded joints with that of Mg/Mg similar joints. The results show that the Mg/steel and the Mg/Mg spot welds have similar fatigue performance. The fatigue strength of Al/steel dissimilar friction spot welds is substantially lower (about half) than that of Al/Al spot joints.[30,36] The main reason for the lower fatigue strength of the Al/steel joint is the brittle Al–Fe IMCs formed at the interfacial region.[36] Mallick and Agrawal[37] compared the fatigue performance of friction spot welds of Mg/Mg, Al/Al and Mg/Al on tensile shear specimens. They showed that Al/Al and Mg/Al had the highest and lowest fatigue strength, respectively. Xu *et al.*[38] compared the microstructure and mechanical behaviour of Mg/steel spot welds with those of weld-bonded Mg/Mg and Mg/steel joints. In both Mg/steel spot welds and Mg/steel weld bonds, fusion zone was formed only at the Mg side, which consists of equiaxed dendrites at the interface and columnar dendrites near the boundary of fusion zone. Static and fatigue tests revealed that the weld-bonded Mg/Mg was stronger than weld-bonded Mg/steel, and both of them were substantially stronger than Mg/steel spot welds. This was related mainly to the high stress concentration at the vicinity of the nugget in the spot weld joints, while the stress distribution in the weld-bonded joints was more uniform. To the authors' knowledge, as of to date, fatigue performance of Mg/Al dissimilar resistance spot welds has not been studied.

This paper, therefore, aimed to characterize the fatigue behaviour of Mg/Al resistance spot welds with Sn-coated steel interlayer. Load-controlled cyclic loads with positive R ratio were applied to spot weld specimens over a wide range of load amplitudes. Failure modes under different cyclic load levels were discussed as well as the crack propagation behaviour. The failure modes were compared with failure modes in Mg/Mg spot welds. The microstructures of the joint cross section and fracture surfaces were analysed by the scanning electron microscope (SEM) and energy-dispersive X-ray analysis (EDS) methods.

MATERIALS AND EXPERIMENTS

AZ31B-H24 magnesium sheet and AA5052-H32 aluminium sheet were used in the current study of dissimilar magnesium to aluminium joining. The AZ31B-H24

Table 1 Composition of the AA5052, AZ31 and Sn-coated steel (in wt%)

Materials	Al	Mg	Fe	Mn	Zn	Si	C	P	S
AA5052	Bal.	2.2-2.8	0.4	0.1	0.1	0.25	—	—	—
AZ31B	2.9	Bal.	—	0.3	1.1	0.01	—	—	—
Steel	—	—	Bal.	0.5	—	—	0.01	0.001	0.005

sheet was strain-hardened and partially annealed, and the AA5052-H32 aluminium sheet was strain-hardened and stabilized. An Sn electroplated, cold-rolled AISI 1008 plain carbon steel sheet (0.6 mm) was used as the interlayer. The thickness of the Sn coating was around 1 μm. The compositions of the as-received materials are shown in Table 1.

Table 2 shows the monotonic tensile properties of the base metals along the rolling direction. The AA5052 and AZ31B sheets have the same thickness of 2 mm and were cut to rectangular coupons of the size 125 × 38 mm along the sheet rolling direction.

Before welding, the coupons were cleaned to prevent porosity and expulsion.[26,39] A solution of 2.5 g chromic oxide in 100 mL water was used for cleaning AZ31B coupons, and a solution of 1.2 mL HF, 67.5 mL HNO_3 and 100 mL water was used for cleaning AA5052 coupons. A Sn-coated steel interlayer with dimensions of 20 × 20 × 0.6 mm was inserted between the Mg and Al coupons before welding. The cleaned coupons were used to make tensile shear specimens according to the specifications of the AWS-D17.2 standard,[40] as shown in Fig. 1. The welding procedure to make the spot-welded specimens was the same as that in the work by Sun *et al.*[27]

Table 2 Tensile properties of the base metals

Materials	0.2% Yield strength (MPa)	Ultimate strength (MPa)	Ductility (%)
AA5052-H32[37]	190	260	12
AZ31-H24[32]	224	292	14

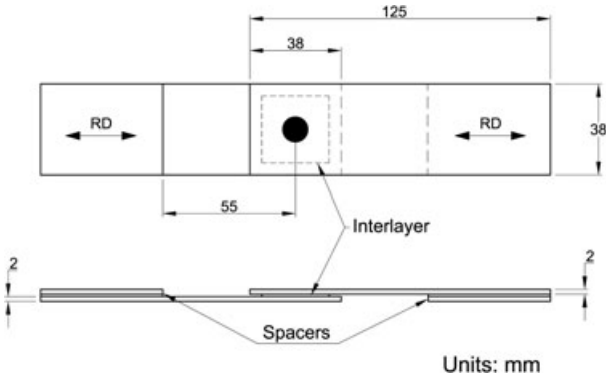

Fig. 1 Spot-welded specimen geometry (dimensions are in mm).

For static and fatigue testing, spacers were used at the two ends of specimens to fill out the coupon offset to prevent additional coupon bending, as shown in Fig. 1. Static and fatigue tests were performed at the room temperature by using a MTS servo hydraulic uniaxial machine with FlexTest controller and ±50 kN axial force capacity. Static testing was conducted in the displacement-controlled mode with the displacement rate of 1 mm min^{-1}. The force and displacement histories as well as the failure mode were recorded in static tests. Fatigue tests were performed under load-controlled mode with a load ratio $R = F_{min}/F_{max} = 0.1$, where F_{min} and F_{max} are minimum and maximum forces, respectively. The waveform for fatigue loading was sinusoidal. Depending on the applied load, the loading frequency was within the range of 2 to 30 Hz, that is, low frequency for high cyclic loads and high frequency for low cyclic loads. Fatigue tests were continued until failure, that is, the separation of coupons, or up to 10 million cycles, considered run-outs. The force and displacement histories, the failure modes and the number of cycles were recorded in fatigue tests.

An Olympus BX51M system optical microscope and JSM 6460 SEM equipped with EDS were used for the microstructure observation of the joint cross section and fracture surfaces. For microstructure analysis from the nugget cross section, the magnesium side fusion zone was revealed by a Nital Etchant, and the aluminium side was etched with a 2% HF solution.

RESULTS AND DISCUSSION

Nugget cross section profile

Figure 2 shows an overview of the cross section of AA5052/AZ31B spot weld with an Sn-coated steel interlayer. As displayed in Fig. 3a, Al–Fe IMCs are formed at the Al/steel interface. According to the literature,[27,41,42] the Al–Fe IMCs are expected to consist of $FeAl_3$ and Fe_2Al_5. The thickness of the IMC layer was about 4 μm at the centre of nugget and reduced to 2 μm towards the edge. At the Mg/steel interface, Fig. 3b, welding occurred because of the existence of the $Al_8(Mn, Fe)_5$

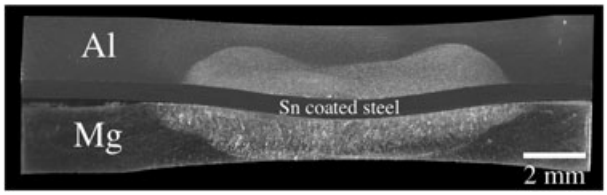

Fig. 2 Typical cross section of Mg/Al dissimilar spot weld with Sn-coated steel interlayer at 36 kA welding current.

layer.[43] Also, squeezed-out Mg–Mg_2Sn eutectic + α-Mg structure[27] was observed in the Mg side fusion zone near the edge of the nugget.

Mechanical properties

Static and fatigue performance of Mg/Al joints is presented and discussed in this section. The mechanical behaviour of Mg/Al spot welds with Sn-coated steel interlayer is compared with those of Mg/Al direct welds (without interlayer). The results for the Mg/Mg spot welds with the same specimen geometry and testing condition were included in the comparison as a benchmark.[33] The comparison requires a reasonable basis, especially because the size of nuggets and coupon offsets are different in the three sets of specimens. To make a meaningful comparison, the strategy was to compare the fatigue strength of different material combinations at the highest static strength. In other words, welding parameters were optimized for each combination, independently to achieve the highest possible static load. The optimized welding process was then employed to make the fatigue specimens.

In earlier studies by the authors, the welding parameters were optimized for Mg/Al spot welds[27] and Mg/Mg spot welds[32] to achieve the maximum static tensile shear load. The optimum welding parameters and average nugget diameters for Mg/Al and Mg/Mg spot welds are summarized in Table 3.

The static performance of Mg/Al and Mg/Mg spot welds is compared in Fig. 4. This demonstrates that the peak loads and ductility in Mg/Al direct welds are significantly lower than those in Mg/Al spot welds with interlayer, although the nugget diameters are very close (Table 3). The poor static performance of Mg/Al direct welds was attributed to brittle Al–Mg IMCs in the fusion zone.[27] In Mg/Al spot welds with interlayer, the Sn-coated steel prevented the formation of the Al–Mg IMCs and resulted in substantial improvement in both the peak load and the ductility. Utilizing the interlayer has made the Mg/Al spot welds to reach to the same level of peak load and ductility as Mg/Mg spot welds.

Figure 5 illustrates the fatigue test results in terms of load-life curve obtained for Mg/Al spot welds with and without the interlayer. The fatigue test results are also listed in Table 4. Mg/Al direct welds exhibited poor

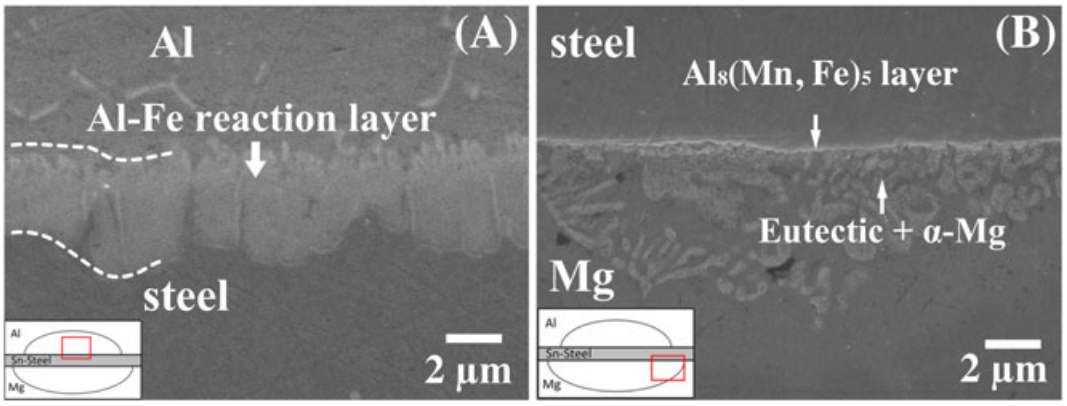

Fig. 3 Microstructure of Mg/Al spot welds with Sn-coated steel interlayer: (a) Al/steel interface and (b) Mg/steel interface. [Colour figure can be viewed at wileyonlinelibrary.com]

Table 3 Optimized welding parameters and weld nugget diameters

Specimen	Welding current (kA)	Welding time (cycle[a])	Electrode force (kN)	Avg. nugget diameter (mm)
Mg/Mg	34	8	4	10.4
Mg/Al direct welding	36	5	4	10.3
Mg/Al with interlayer	36	5	4	10.0[b]

[a]1 cycle = 1/60 s (power frequency = 60Hz).
[b]For Mg/Al spot welds with interlayer, the nugget diameter was measured from the Al/steel interface where failure occurred in static tests.

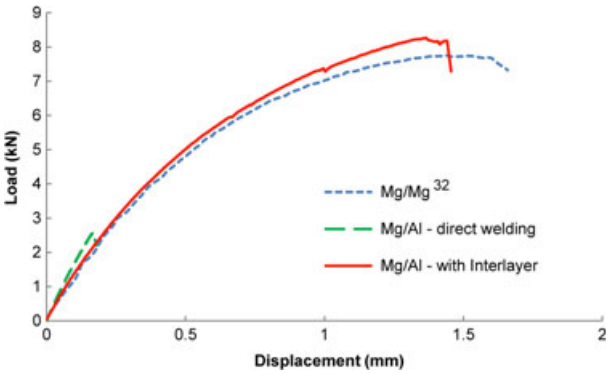

Fig. 4 Typical load displacement static test results for Mg/Al and Mg/Mg spot welds. [Colour figure can be viewed at wileyonlinelibrary.com]

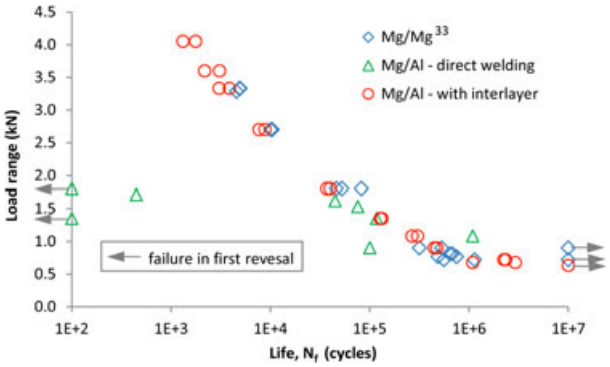

Fig. 5 Fatigue performance of Mg/Al and Mg/Mg spot welds. [Colour figure can be viewed at wileyonlinelibrary.com]

fatigue strength especially in the LCF regime, which was expected from the low static strength of these welds, as shown in Fig. 4 and as reported in an earlier study.[27] Failure in all Mg/Al direct welds occurred through nugget at the interface, showing very scattered fatigue strengths. Non-repeatable results of Mg/Al direct welds limit the reliability of the results for a worthwhile comparison between Mg/Al direct welds and other two welds. Adding the Sn-coated steel interlayer, however, recovered the fatigue strength to the same level as Mg/Mg spot welds. For Mg/Al spot welds with interlayer, the increase in the cross-head displacement amplitude versus loading cycles is shown in Fig. 6 and is compared with that for Mg/Mg welds under the same load ranges, ΔF. The figure includes the results for different life spans, from low to mid and HCF. This graph demonstrates that during the load-controlled fatigue tests, the cross-head displacement amplitude is relatively constant at the beginning but gradually increases, and the rate of change drastically rises towards the end of the test.

The increase in the displacement amplitude is an indication of specimen properties' degradation, that is, loss of the specimen's stiffness due to crack initiation and propagation. The onset of the rise in the displacement amplitude is an evidence of the fatigue crack initiation at the nugget edge, and the rapid increase in the slope represents the domain of the fatigue crack propagation leading to the final failure. As depicted by Fig. 6, for

Table 4 Fatigue test results for Mg/Al spot welds with and without interlayer and comparison with Mg/Mg spot welds

Mg/Mg		Mg/Al direct welding		Mg/Al with interlayer	
Load range [kN]	Life (cycle)	Load range [kN]	Life (cycle)	Load range [kN]	Life (cycle)
3.33	4873	1.8	1	4.05	1767
3.33	4958	1.71	447	4.05	1317
3.29	4563	1.62	44 756	3.6	3070
2.70	10 131	1.53	75 760	3.6	2173
2.70	10 472	1.35	3	3.33	3052
2.70	10 068	1.35	117 280	3.33	3857
1.80	52 384	1.08	1 090 056	2.7	7691
1.80	82 240	0.9	100 254	2.7	8793
1.80	46 221			1.8	37 170
0.90	316 298			1.8	40 054
0.90	531 352			1.35	128 088
0.90	>10 000 000			1.35	132 959
0.81	641 537			1.08	267 328
0.81	679 549			1.08	303 603
0.77	486 572			0.9	446 476
0.77	751 491			0.9	475 559
0.72	558 984			0.72	2 343 916
0.72	1 136 069			0.72	2 241 679
0.72	>10 000 000			0.675	2 924 368
				0.675	1 092 087
				0.63	>10 000 000

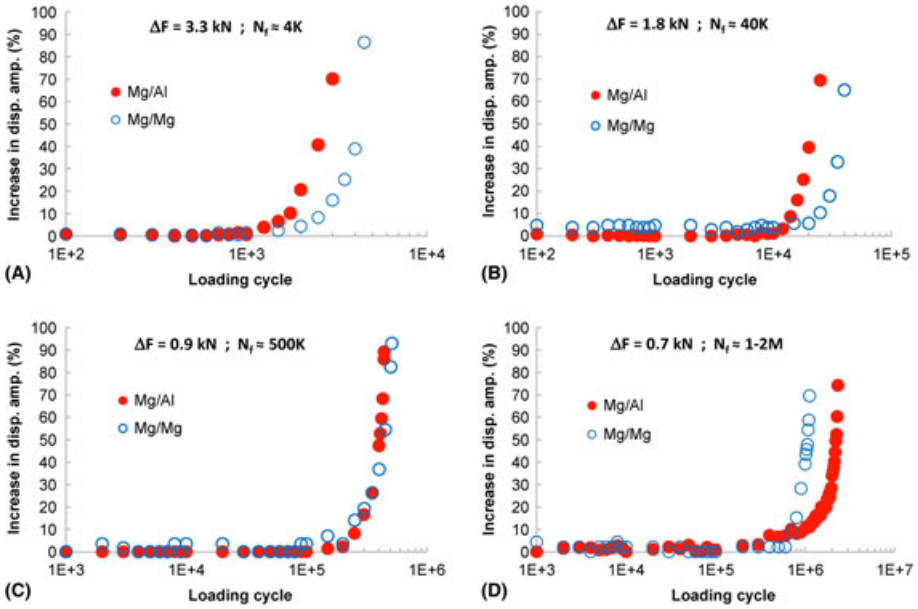

Fig. 6 Increase in displacement amplitude for Mg/Al and Mg/Mg spot welds under different cyclic loading. [Colour figure can be viewed at wileyonlinelibrary.com]

the life range of $N_f < 10^5$ cycles (Fig. 6a and b), Mg/Al specimens degrade earlier than Mg/Mg welds, resulting in shorter lives for Mg/Al welds. However, at higher lives with $N_f > 10^5$ cycles (Fig. 6c and d), the trend in the load-life behaviour for Mg/Mg is a plateau (Fig. 5), meaning that a Mg/Mg spot weld may have a finite life, for example, $N_f = 5 \times 10^5$ cycles, or an 'infinite' life, that is, $N_f > 10^7$ cycles under a slightly different load range. Therefore, a meaningful comparison cannot be made between the degradation rates of Al/Mg and Mg/Mg, within this life range. The earlier weld degradation and failure in Mg/Al joints, as shown in Fig. 6a and b for fatigue lives $N_f < 10^5$, may be attributed to the existence of interlayer that results in increased bending moment and higher stress levels.

The degradation rate for Mg/Mg welds for $N_f > 10^5$ cycles, contrary to lives $N_f < 10^5$, is similar to or faster than Mg/Al (Fig. 6c and d), while stresses in Mg/Al

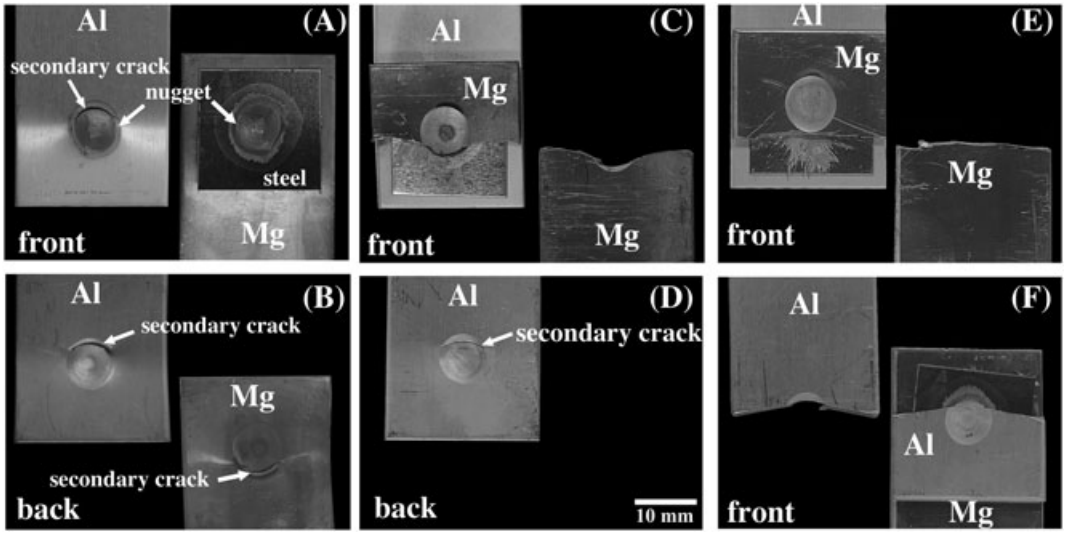

Fig. 7 Fatigue failure modes for the Mg/Al specimens: (a) and (b) front and back of failed specimen subjected to a high cyclic load, $\Delta F = 3.3$ kN; (c) and (d) front and back of failed specimen subjected to an intermediate cyclic load, $\Delta F = 1.8$ kN; (e) specimen subjected to a low cyclic load, $\Delta F = 0.7$ kN with failure at Mg side; (f) specimen subjected to a low cyclic load, $\Delta F = 0.7$ kN with failure at Al side.

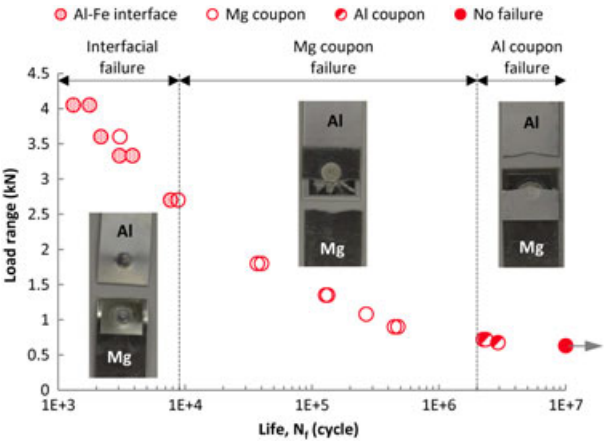

Fig. 8 Different failure modes in Mg/Al dissimilar welds. [Colour figure can be viewed at wileyonlinelibrary.com]

remain larger than Mg/Mg. Within the $N_f > 10^5$ cycles, as displayed by Fig. 5, the load-life curve for Mg/Mg welds exhibits a plateau. This can be attributed to the fatigue behaviour of AZ31B sheet, because fatigue cracks in spot-welded specimens initiate and propagate in the base metal (away from the weld), within the HCF regime.[32] Fatigue strength of AZ31B sheet reaches a plateau around the life of 10^5 cycles.[44,45] This means that a slight change in the stress level within this regime may result in a finite life or no failure up to $N_f = 10^7$. Hence, the degradation behaviour for Mg/Mg welds for $N_f > 10^5$ cycles (Fig. 6c and d) where the stress levels are low may be attributed to the plateau nature of fatigue behaviour of Mg.

Failure modes

Three different failure modes of the Mg/Al joints with Sn-coated steel interlayer were observed under cyclic loading: interfacial failure, coupon failure on Mg side and coupon failure on Al side. Failure mode in Mg/Al spot welds with interlayer depended strongly on the fatigue loading condition.

Interfacial failure occurred in specimens subjected to large cyclic loads (load range, $\Delta F > 2.7$ kN). Figure 7a shows a typical failure in a specimen subjected to a cyclic load with $\Delta F = 3.3$ kN. High cyclic loads cause severe bending in coupons, which makes the interfacial plane more critical than the plane normal to the loading direction. Therefore, interfacial failure is common under high cyclic loads.[32] Along with the major failure at the Al/steel interface, secondary cracks were propagated through the coupon thickness on both Al and Mg coupons close to the nugget edge, which is depicted in Fig. 7a and b. The Al/steel interfacial failure indicates that steel creates better bonding with magnesium than with aluminium.[27]

Coupon failure occurred in welded specimens subjected to cyclic loading of intermediate and low amplitudes. When the load range was between 0.9 and 2.7 kN, that is, the life was within the range of $10^4 < N_f < 2 \times 10^6$ cycles, primary crack initiated at the nugget edge and propagated in the Mg coupon, while secondary crack was observed in the Al coupon, as shown in Fig. 7c and d.

Specimens subjected to very low cyclic loading ($\Delta F < 0.9$ kN) demonstrated a transition from Mg coupon failure to Al coupon failure, as displayed in Fig. 7e and f. More investigation is needed to explain the transition in the fatigue failure mode. Figure 8 depicts different failure modes of Mg/Al spot welds with interlayer.

Fracture surfaces

Mg/Al direct welds

Figure 9 shows the typical fatigue fracture surfaces of Mg/Al direct welds. Unlike the various failure modes of the Mg/Al-welded specimens with interlayer, all of the Mg/Al direct welds failed at the Mg/Al interface through the nugget, as shown in Fig. 9a. Similar failure

Table 5 EDS analyses results (at%) for the regions shown in Figs. 9 and 10

Spectrum	Mg	Al	Fe
1	48.9	51.1	—
2	58.9	41.1	—
3	0.2	81.4	18.4
4	2.3	97.7	—

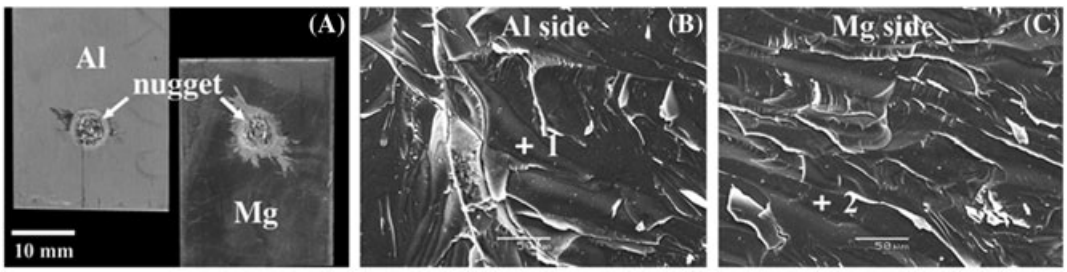

Fig. 9 Typical fatigue fracture of Mg/Al direct weld: (a) failure mode, (b) fracture surface in Al side and (c) fracture surface in Mg side; points 1 and 2 are for EDS analyses, the results of which are shown in Table 5.

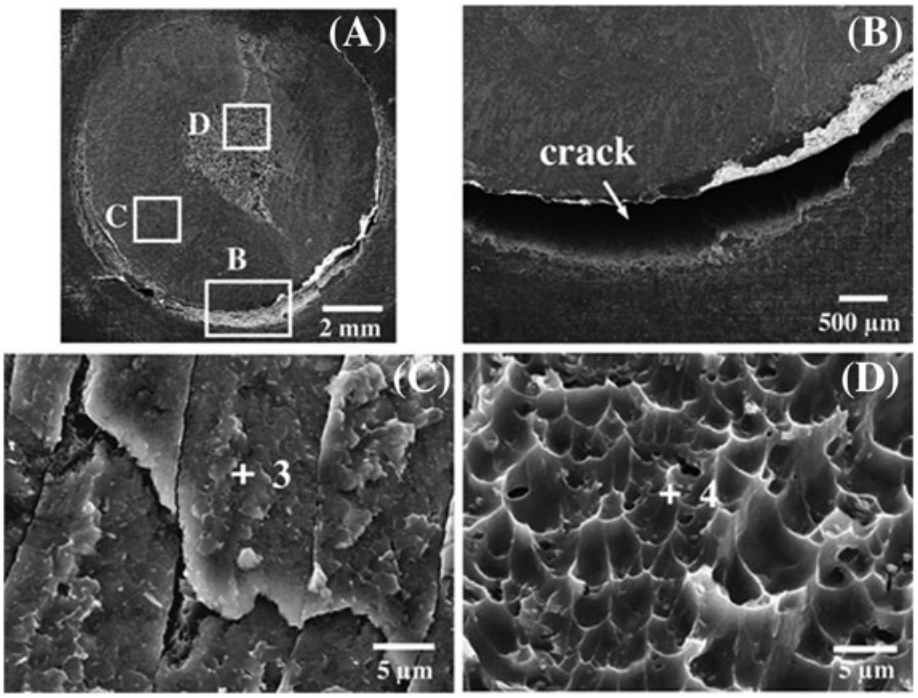

Fig. 10 Fatigue fracture in Mg/Al joints with Sn-coated steel interlayer, under $\Delta F = 3.3$ kN: (a) fractured nugget in Al side, (b) secondary crack in Al coupon, (c) fatigue crack propagation region and (d) final rupture region; points 3 and 4 are for EDS analyses, shown in Table 5.

mode was observed in Mg/Al direct welds under static tensile shear loading, in the present and previous studies.[27] The SEM images in Fig. 9b and c demonstrate brittle fracture in the nugget of Mg/Al direct welds. The EDS analysis results, presented in Table 5 (spectra 1 and 2) revealed that the Al–Mg IMCs are present on the fracture surface. The low strength, premature nugget failure, and the brittle morphology of the fracture surface can be attributed to the formation of hard and brittle Al–Mg IMCs, such as Al_3Mg_2 and $Al_{12}Mg_{17}$, inside the nugget.[7,11,18]

Mg/Al welds with interlayer

Figure 10 displays the fatigue fracture surface of Mg/Al welds with Sn-coated steel interlayer, under a high cyclic load, $\Delta F = 3.3$ kN, which resulted in Al/steel interfacial failure. Figure 10a shows the fracture surface in Al side, and Fig. 10b displays a secondary crack through the Al coupon thickness, region B in Fig. 10a. SEM examination on the fracture surface (Fig. 10c and d) revealed two different morphologies on the fracture surface: region C with brittle morphology representative of fatigue crack

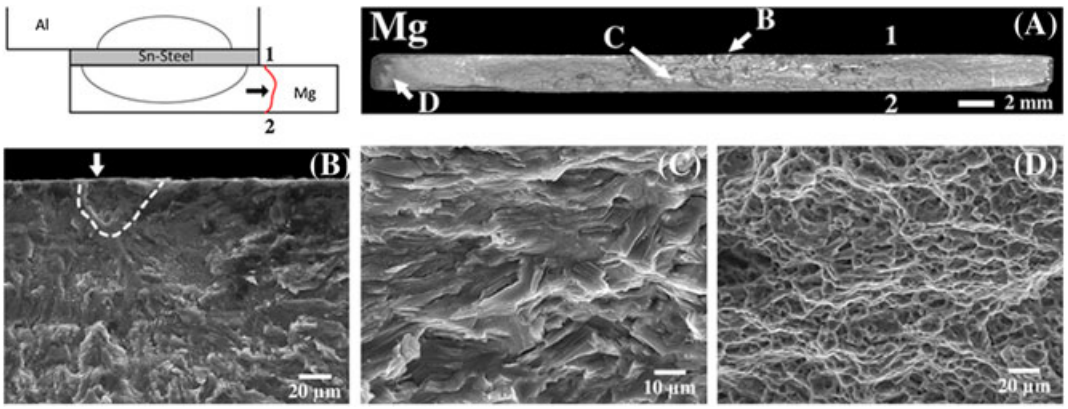

Fig. 11 Fatigue fracture in Mg/Al joints with Sn-coated steel interlayer, Mg sheet, under $\Delta F = 0.7$ kN: (a) fracture surface overview, (b) location of fatigue crack initiation (region B as marked in panel a), (c) crack propagation region (C as marked in panel a) and (d) final fracture (region D in panel a). [Colour figure can be viewed at wileyonlinelibrary.com]

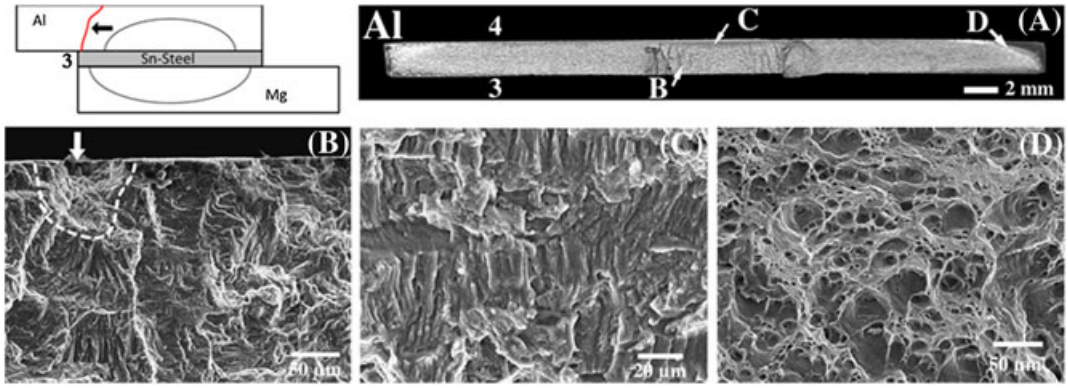

Fig. 12 Fatigue fracture in Mg/Al joints with Sn-coated steel interlayer, Al sheet, under $\Delta F = 0.7$ kN: (a) fracture surface overview, (b) location of fatigue crack initiation (region B as marked in panel a), (c) crack propagation region (C as marked in panel a) and (d) final fracture (region D in a). [Colour figure can be viewed at wileyonlinelibrary.com]

propagation and region D with dimpled morphology indicative of final rupture.

Elemental analysis with EDS demonstrated that region C contains both Al and Fe elements (spectrum 3 in Table 5), while region D contains only Al (spectrum 4 in Table 5). This observation suggests that fatigue crack propagation occurred in Al–Fe IMCs and final rupture inside the Al fusion zone. The brittle structure of the Al–Fe reaction layer made this region favourable for crack propagation. Similar observation was made in fatigue failure of Al/steel welds, that is, fatigue crack initiated and propagated at Al/steel interface within the Al–Fe intermetallic layer.[46]

Figures 11 and 12 show typical fracture surfaces in the specimens failed in Mg and Al coupons, respectively. In either case, fatigue crack initiated at the sheet surface close to the nugget edge (Figs. 11b and 12b) and afterwards propagated towards the thickness. Figures 11c and 12c show the fatigue propagation region with brittle morphology. Figures 11d and 12d show ductile fracture in the final rupture region. Similar observations were made at the fatigue fracture surface of Mg/Mg joint.[35]

CONCLUSIONS

The focus in this research was on fatigue characterization and failure modes of AA5052 to AZ31B dissimilar resistance spot welds with Sn-coated steel interlayer. The conclusions made from this study are as follows:

1. The fatigue results of the Mg/Al joints with Sn-coated steel interlayer show comparable fatigue strength to that of Mg/Mg similar welds.
2. Within the life range of $N_f < 10^5$, fatigue degradation rate is higher in the Mg/Al welds than in Mg/Mg welds; therefore, the fatigue life for Mg/Al welds is shorter than that for Mg/Mg welds. This behaviour was attributed to the existence of an interlayer between the two coupons, which adds to the coupon offset and bending moment in the Mg/Al welds.
3. Three failure modes were observed in the Mg/Al joints with Sn-coated steel interlayer under different levels of cyclic loading: Al/steel interfacial failure, Mg coupon failure and Al coupon failure. However, interfacial failure was the only mode of fatigue failure in Mg/Al direct welds.
4. Failure in LCF regime (fatigue life $N_f < 10^4$ cycles) occurred at Al/steel interfacial region. This observation indicates that steel creates better bonding with Mg than with Al, under the welding conditions studied in the present research. In the HCF regime (up to $N_f < 2 \times 10^6$ cycles), failure occurred in Mg coupon, while at longer lives, Al coupon failure was observed.
5. Fatigue fracture surface of Mg/Al direct weld had brittle morphology, which was attributed to the brittle Al–Mg intermetallics in the fusion zone. For Mg/Al welds with interlayer, under high cyclic loading, fatigue crack propagated in Al–Fe IMCs leaving a brittle fracture surface, while the final rupture was in ductile mode. Similarly, under low cyclic loading, fatigue crack propagation and final rupture regions had brittle and ductile morphologies, respectively.

Acknowledgements

The authors would like to acknowledge the financial supports by the Natural Sciences and Engineering Research Council (NSERC), Automotive Partnership

Canada (APC), NSERC Magnesium Network (MagNET) and the State Scholarship Fund of China (No. 201206120134). Also, the authors appreciate Dr S.T. Niknejad for his help with SEM analyses, K. Troung for his help with cyclic tests and Dr M.K. Lee for the supply of magnesium sheets.

REFERENCES

1 Schubert, E., Klassen, M., Zerner, I., Walz, C. and Sepold, G. (2001) Light-weight structures produced by laser beam joining for future applications in automobile and aerospace industry. *J. Mater. Process. Technol.*, **115**, 2–8.
2 Liu, L., Ren, D. and Liu, F. (2014) A review of dissimilar welding techniques for magnesium alloys to aluminum alloys. *Materials*, **7**, 3735–3757.
3 Çam, G. and Koçak, M. (1998) Progress in joining of advanced materials. *Int. Mater. Rev.*, **43**, 1–44.
4 Liu, L., Liu, X. and Liu, S. (2006) Microstructure of laser-TIG hybrid welds of dissimilar Mg alloy and Al alloy with Ce as interlayer. *Scr. Mater.*, **55**, 383–386.
5 Chowdhury, S., Chen, D., Bhole, S., Cao, X. and Wanjara, P. (2013) Lap shear strength and fatigue behavior of friction stir spot welded dissimilar magnesium-to-aluminum joints with adhesive. *Mater. Sci. Eng. A*, **562**, 53–60.
6 ASM (1992) Alloy phase diagrams, Al (aluminum) binary alloy phase diagrams. *Asm Int.*, **2**, 4–2.56.
7 Borrisutthekul, R., Miyashita, Y. and Mutoh, Y. (2005) Dissimilar material laser welding between magnesium alloy AZ31B and aluminum alloy A5052-O. *Sci. Technol. Adv. Mater.*, **6**, 199–204.
8 Liu, L. and Wang, H. (2011) Microstructure and properties analysis of laser welding and laser weld bonding Mg to Al joints. *Metall. Mater. Trans. A.*, **42**, 1044–1050.
9 Shang, J., Wang, K.-h., Qi, Z., D-k, Z., Huang, J. and J-q, G. (2012) Effect of joining temperature on microstructure and properties of diffusion bonded Mg/Al joints. *Trans. Nonferrous Met. Soc. Chin.*, **22**, 1961–1966.
10 Dietrich, D., Nickel, D., Krause, M., Lampke, T., Coleman, M. and Randle, V. (2011) Formation of intermetallic phases in diffusion-welded joints of aluminium and magnesium alloys. *J. Mater. Sci.*, **46**, 357–364.
11 Liu, P., Li, Y., Geng, H. and Wang, J. (2007) Microstructure characteristics in TIG welded joint of Mg/Al dissimilar materials. *Mater. Lett.*, **61**, 1288–1291.
12 Luo, Y. and Li, J. (2014) Analysis of nugget formation during resistance spot welding on dissimilar metal sheets of aluminum and magnesium alloys. *Metall. Mater. Trans. A.*, **45**, 5107–5113.
13 Patel, V., Bhole, S. and Chen, D. (2012) Microstructure and mechanical properties of dissimilar welded Mg-Al joints by ultrasonic spot welding technique. *Sci. Technol. Weld. Joining*, **17**, 202–206.
14 Robson, J., Panteli, A. and Prangnell, P. (2012) Modelling intermetallic phase formation in dissimilar metal ultrasonic welding of aluminium and magnesium alloys. *Sci. Technol. Weld. Joining*, **17**, 447–453.
15 Firouzdor, V. and Kou, S. (2010) Al-to-Mg friction stir welding: effect of material position, travel speed, and rotation speed. *Metall. Mater. Trans. A.*, **41**, 2914–2935.
16 Sato, Y. S., Park, S. H. C., Michiuchi, M. and Kokawa, H. (2004) Constitutional liquation during dissimilar friction stir welding of Al and Mg alloys. *Scr. Mater.*, **50**, 1233–1236.
17 Venkateswaran, P. and Reynolds, A. P. (2012) Factors affecting the properties of friction stir welds between aluminum and magnesium alloys. *Mater. Sci. Eng. A*, **545**, 26–37.
18 Hayat, F. (2011) The effects of the welding current on heat input, nugget geometry, and the mechanical and fractural properties of resistance spot welding on Mg/Al dissimilar materials. *Mater. Design*, **32**, 2476–2484.
19 Rao, H., Yuan, W. and Badarinarayan, H. (2015) Effect of process parameters on mechanical properties of friction stir spot welded magnesium to aluminum alloys. *Mater. Design*, **66**, 235–245.
20 Liu, L.-M., Wang, H.-Y. and Zhang, Z.-D. (2007) The analysis of laser weld bonding of Al alloy to Mg alloy. *Scr. Mater.*, **56**, 473–476.
21 Penner, P., Liu, L., Gerlich, A. and Zhou, Y. (2014) Dissimilar resistance spot welding of aluminum to magnesium with Zn coated steel interlayers. *Weld J.*, **93**, 225s–231s.
22 X-d, Q. and L-m, L. (2012) Fusion welding of Fe-added lap joints between AZ31B magnesium alloy and 6061 aluminum alloy by hybrid laser–tungsten inert gas welding technique. *Mater. Design*, **33**, 436–443.
23 Zhao, L. and Zhang, Z. (2008) Effect of Zn alloy interlayer on interface microstructure and strength of diffusion-bonded Mg–Al joints. *Scr. Mater.*, **58**, 283–286.
24 Gao, M., Mei, S., Li, X. and Zeng, X. (2012) Characterization and formation mechanism of laser-welded Mg and Al alloys using Ti interlayer. *Scr. Mater.*, **67**, 193–196.
25 Song, G., An, G. and Liu, L. (2012) Effect of gradient thermal distribution on butt joining of magnesium alloy to steel with Cu–Zn alloy interlayer by hybrid laser–tungsten inert gas welding. *Mater. Design*, **35**, 323–329.
26 Penner, P., Liu, L., Gerlich, A. and Zhou, Y. (2013) Feasibility study of resistance spot welding of dissimilar Al/Mg combinations with Ni based interlayers. *Sci. Technol. Weld. Joining*, **18**, 541–550.
27 Sun, M., Niknejad, S., Gao, H., Wu, L. and Zhou, Y. (2016) Mechanical properties of dissimilar resistance spot welds of aluminum to magnesium with Sn-coated steel interlayer. *Mater. Design*, **91**, 331–339.
28 Sun, M., Niknejad, S., Zhang, G., Lee, M., Wu, L. and Zhou, Y. (2015) Microstructure and mechanical properties of resistance spot welded AZ31/AA5754 using a nickel interlayer. *Mater. Design*, **87**, 905–913.
29 Vural, M., Akkus, A. and Eryurek, B. (2006) Effect of welding nugget diameter on the fatigue strength of the resistance spot welded joints of different steel sheets. *J. Mater. Process. Technol.*, **176**, 127–132.
30 Chang, B. H., Du, D., Sui, B., Zhou, Y., Wang, Z. and Heidarzadeh, F. (2007) Effect of forging force on fatigue behavior of spot welded joints of aluminum alloy 5182. *J. Manuf. Sci. Eng.*, **129**, 95–100.
31 Behravesh, S. B., Liu, L., Jahed, H., Lambert, S., Glinka, G. and Zhou, Y. (2010) Effect of nugget size on tensile and fatigue strength of spot welded AZ31 magnesium alloy. *SAE World Congress & Exhibition* (*SAE Technical Paper*: *2010-01-0411*), Detroit, Michigan, United States.
32 Behravesh, S. B., Jahed, H. and Lambert, S. (2011) Characterization of magnesium spot welds under tensile and cyclic loadings. *Mater. Design*, **32**, 4890–4900.
33 Behravesh, S. B., Jahed, H. and Lambert, S. (2014) Fatigue characterization and modeling of AZ31B magnesium alloy spot-welds. *Int. J. Fatigue*, **64**, 1–13.

34 Xiao, L., Liu, L., Chen, D., Esmaeili, S. and Zhou, Y. (2011) Resistance spot weld fatigue behavior and dislocation substructures in two different heats of AZ31 magnesium alloy. *Mater. Sci. Eng. A*, **529**, 81–87.
35 Liu, L., Xiao, L., Chen, D., Feng, J., Kim, S. and Zhou, Y. (2013) Microstructure and fatigue properties of Mg-to-steel dissimilar resistance spot welds. *Mater. Design*, **45**, 336–342.
36 Tran, V.-X. and Pan, J. (2010) Fatigue behavior of dissimilar spot friction welds in lap-shear and cross-tension specimens of aluminum and steel sheets. *Int. J. Fatigue*, **32**, 1167–1179.
37 Park, S., Lee, C. G., Kim, J., Han, H. N., Kim, S.-J. and Chung, K. (2008) Improvement of formability and spring-back of AA5052-H32 sheets based on surface friction stir method. *J. Eng. Mater. Technol.*, **130**, 041007.
38 Xu, W., Chen, D., Liu, L., Mori, H. and Zhou, Y. (2012) Microstructure and mechanical properties of weld-bonded and resistance spot welded magnesium-to-steel dissimilar joints. *Mater. Sci. Eng. A*, **537**, 11–24.
39 Liu, L., Xiao, L., Feng, J. C., Tian, Y. H., Zhou, S. Q. and Zhou, Y. (2010) The mechanisms of resistance spot welding of magnesium to steel. *Metall. Mater. Trans. A*, **41A**, 2651–2661.
40 American Welding Society (2007) *Specification for Resistance Welding for Aerospace Applications*, AWS Standard: Miami, FL, United States.
41 Qiu, R., Shi, H., Zhang, K., Tu, Y., Iwamoto, C. and Satonaka, S. (2010) Interfacial characterization of joint between mild steel and aluminum alloy welded by resistance spot welding. *Mater Charact*, **61**, 684–688.
42 Qiu, R., Iwamoto, C. and Satonaka, S. (2009) Interfacial microstructure and strength of steel/aluminum alloy joints welded by resistance spot welding with cover plate. *J. Mater. Process. Technol.*, **209**, 4186–4193.
43 Nasiri, A., Weckman, D. and Zhou, Y. (2015) Interfacial microstructure of laser brazed AZ31B magnesium to SnPlated steel sheet. *Weld J.*, **94**, 61s–72s.
44 Morita, S., Ohno, N., Tamai, F. and Kawakami, Y. (2010) Fatigue properties of rolled AZ31B magnesium alloy plate. *Trans. Nonferrous Met. Soc. Chin.*, **20**, s523–s526.
45 Behravesh, S. B. (2013) Fatigue characterization and cyclic plasticity modeling of magnesium spot joints. *Mechanical Engineering*. University of Waterloo.
46 Patel, V., Bhole, S. and Chen, D. (2014) Ultrasonic spot welding of aluminum to high-strength low-alloy steel: microstructure, tensile and fatigue properties. *Metall. Mater. Trans. A.*, **45**, 2055–2066.